

Bandgap engineering of zigzag graphene nanoribbons by manipulating edge states via defective boundaries

Aihua Zhang¹, Yihong Wu³, San-Huang Ke⁴, Yuan Ping Feng¹, Chun Zhang^{1,2*}

¹*Department of Physics, National University of Singapore,*

2 Science Drive 3, Singapore 117542

²*Department of Chemistry, National University of Singapore,*

3 Science Drive 3, Singapore 117543

³*Department of Electrical and Computer Engineering,*

National University of Singapore, 4 Engineering Drive 3, Singapore, 117576

⁴*Department of Physics, Tongji University,*

1239 Siping Road, Shanghai 200092, P. R. China

(Dated: November 12, 2018)

Abstract

One of severe limits of graphene nanoribbons (GNRs) in future applications is that zigzag GNRs (ZGNRs) are gapless, so cannot be used in field effect transistors (FETs). In this paper, using tight-binding approach and first principles method, we derived and proved a general edge (boundary) condition for the opening of a significant bandgap in ZGNRs with defective edge structures. The proposed semiconducting GNRs have some interesting properties including the one that they can be embedded and integrated in a large piece of graphene without the need of completely cutting them out. We also demonstrated a new type of high-performance all-ZGNR FET.

I. INTRODUCTION

Graphene has attracted intensive research efforts due to its unique electronic and mechanical properties.¹⁻³ A recent experiment demonstrated a beautiful technique in fabricating graphene nanoribbons (GNRs) with atomically precise edges, suggesting the great potential of GNRs in future applications of graphene-based high performance electronics.⁴ Theoretical calculations showed that only two thirds of armchair graphene nanoribbons (AGNRs) with different widths are semiconducting, while zigzag graphene nanoribbons (ZGNRs) are gapless due to localized edge states at the Fermi level.^{5,6} It was also theoretically demonstrated that these bandgap-closing edge states survive in zigzag GNRs with a mixture of zigzag and armchair sites at boundaries.^{5,7} Another recent theoretical work proved that the confinement by *minimal* boundaries generally does not produce an insulating GNR except for the armchair case.⁸ This theoretically predicted edge or orientation and width dependence of bandgap opening in GNRs provide serious limits in real applications of GNR-based electronic devices: First, gapless ZGNRs cannot be used in FETs, and second, the precise control of the width of AGNRs is required.

In this paper, using the tight-binding approach and the first principles method based on density functional theory (DFT), we derived and proved that when the number of A-site defects equals to that of B-site defects at each boundary (A, B denotes two sublattices of graphene), localized edge states in GNRs will be eliminated, and then a bandgap that is inversely proportional to the ribbon width will generally be open. We then showed that ZGNRs with defective boundaries that satisfy the bandgap opening conditions can be embedded and integrated in a large piece of graphene, which may have implications for the future design of graphene-based integrated circuits. At last, we demonstrate a new type of field effect transistor completely made of ZGNRS. Note that in all previously theoretically proposed GNR-based transistors,⁹ the AGNR is indispensable. It is worthy mentioning here that since the long-range magnetic order is not stable in one-dimensional systems

under finite temperature, we therefore stick to the non-magnetic case in this study.

II. RESULTS AND DISCUSSION

We first focus on a ZGNR with an edge structure with defects as shown in Fig. 1(a). The edge structure can be specified by a quadruple of segment lengths in unit of the graphene lattice constant ($a = 2.46 \text{ \AA}$), $(N_{B,1}, N_{A,1}, N_{B,2}, N_{A,2})$. So the number of two-coordinated carbon atoms at edge belong to A (B) sublattice, N_A (N_B), equals to $N_{A,1} + N_{A,2}$ ($N_{B,1} + N_{B,2}$). The electronic structure was calculated using the tight-binding approach. Only the nearest-neighbor hopping energy (-2.7 eV) was taken into account. It is well known that there exist edge states with $E = 0$ for a semi-infinite graphene with a zigzag edge if $2\pi/3 < k_y a \leq \pi$. The edge state entirely localizes at edge for $k_y a = \pi$, and otherwise decays exponentially away from the edge.⁵ When two zigzag edges form a ZGNR and the edge states from both edges interact with each other, the edge states still degenerate at $k_y a = \pi$, while a small gap that decreases exponentially with the nanoribbon width opens elsewhere. The band structure of a perfect ZGNR in a supercell corresponding to $(9, 0, 0, 0)$ is reproduced in Fig. 1(b). Due to band folding, there are six bands (marked as red) corresponding to $2\pi/3 < k_y a \leq \pi$. We find that these bands originating from edge states are removed and thus an energy gap opens if $N_A = N_B$. An example of the band structure corresponding to a $(3, 3, 3, 3)$ edge structure is shown in Fig. 1(c), and the squared wave functions in the inset clearly indicate they are extended states with the form, $\sin(k_n x)$, which has more nodes for larger energies. Therefore, the energy of the valence band maximum (VBM), hence the energy gap, is inversely proportional to the nanoribbon width. For the case of either $N_A < N_B$ or $N_A > N_B$, some of the edge states will remain as shown in Figs. 1(d) and 1(e), though the perfectly localized edge state is destroyed. The squared wave functions in the insets of Figs. 1(d) and 1(e) show the edge states are exponentially decaying away from the edge, so the energy gap due to the interaction between the states at

opposite edges also decreases exponentially with respect to the nanoribbon width. These two distinct behaviors of the bandgap variation as a function of the nanoribbon width can be seen in Fig. 2(a). The variation of bandgaps with respect to the characteristic length of the edge structure is shown in Fig. 2(b). The possibility to tune bandgaps with different edge structures on the same nanoribbon might provide useful implication in the design of nanoribbon-based electronic devices.

The above mentioned condition for the elimination of edges states that leads to bandgap opening can be understood from the following arguments. Considering a semi-infinite graphene sheet with N_A^e (N_B^e) two-coordinated carbon atoms at the edge and N_A^b (N_B^b) three-coordinated carbon atoms in the bulk belonging to A (B) sublattice, we have the following equation by the conservation of coordinate numbers,

$$2N_A^e + 3N_A^b = 2N_B^e + 3N_B^b.$$

Since the total number of carbon atoms in each sublattice is $N_{A(B)}^t = N_{A(B)}^e + N_{A(B)}^b$, the above equation can be rewritten as $3(N_A^t - N_B^t) = N_A^e - N_B^e$, which means the relation between N_A^t and N_B^t is the same as that between N_A^e and N_B^e . The band structure of graphene in the tight-binding approximation is calculated by

$$E\psi_A(\mathbf{r}) = t[\psi_B(\mathbf{r}) + \psi_B(\mathbf{r} - \mathbf{R}_1) + \psi_B(\mathbf{r} - \mathbf{R}_2)] \quad (1)$$

$$E\psi_B(\mathbf{r}) = t[\psi_A(\mathbf{r}) + \psi_A(\mathbf{r} + \mathbf{R}_1) + \psi_A(\mathbf{r} + \mathbf{R}_2)], \quad (2)$$

where t is the hopping energy, $\psi_A(\mathbf{r})$ and $\psi_B(\mathbf{r})$ are the wave functions on A and B atoms belonging to the same unit cell at a discrete coordinate \mathbf{r} , and \mathbf{R}_1 and \mathbf{R}_2 are graphene lattice vectors as shown in Fig. 1(a). For $E = 0$, Eqs. 1 and 2 are decoupled. There are N_A^t equations with N_B^t unknowns for 1 and N_B^t equations with N_A^t unknowns for 2. So if $N_A^t > N_B^t$, 1 will have no solution while 2 will have solutions on A sublattice. Similar conclusion will arrive for $N_A^t < N_B^t$. The fact that the wave function will reside on the sublattice with more atoms can be observed by comparison of the insets in Figs. 1(d)

and 1(e). If $N_A^t = N_B^t$ and the break of symmetry leads to no linear dependence among equations, then Eqs. 1 and 2 will have only zero solution, which is not admissible and results in the elimination of localized states with $E = 0$ that decay exponentially from the edge. From the above arguments, it can be seen that this boundary condition is a necessary condition for opening bandgaps in GNRs that scale inversely with the width instead of exponentially. Our test calculations also show that this boundary condition of bandgap opening also applies for many other nanoribbons with general orientations and defective edge structures.

In practice, disorders are inevitable in the fabrication of GNRs that involves in the lithographic patterning and etching. We therefore considered a disordered edge structure as shown in Fig. 4: A ZGNR with one (3, 3, 2, 3) unit (as shaded in the figure) plus 10 (3, 3, 3, 3) units in one supercell. Here, the (3, 3, 2, 3) unit can be treated as a disorder in the (3, 3, 3, 3) edge structure. Our tight-binding calculations show that the disorder will induce localized states inside the bandgap (as shown in the figure) that may not contribute to transport, and compared to the edge structure without the disorder, the energy gap between extended states in the disordered structure is bigger than the bandgap of the perfect one. In real experiments, statistically speaking, the gap-opening boundary condition is always satisfied, so our findings presented here may have implications for recent experiments showing that the transport gap of GNRs is inversely proportional to the width, and independent on the orientations or edges of GNRs.¹⁰

An interesting property of nanoribbons with a bandgap-opening edge structure is that if a wide nanoribbon is joined with a narrow nanoribbon, the electronic structure of the wide nanoribbon near the Fermi energy is not altered with electrons still confined in the wide nanoribbon. An example of a nanoribbon with a width of $L = 12\sqrt{3}a$ and a (3, 3, 3, 3) edge structure joined with a nanoribbon with the same edge structure and a width of $L = 5\sqrt{3}a$ is shown in Fig. 3(a). The band structure of the compound system near the Fermi energy (the conduction and valence band) in Fig. 3(b) is almost the same as that

of the stand-alone nanoribbon shown in Fig. 1(c). The charge distribution of the state at VBM in Fig. 3(a) and the local density of states in Fig. 3(c) clearly indicate that the wave function is only localized in the wide nanoribbon. The confinement can be understood from the bandgap difference of two nanoribbons with different widths. Note that the integrated GNRs discussed here can be also regarded as a special type of graphene antidot lattice structures proposed earlier.^{11,12} This property makes it possible to fabricate individual nanoribbon-based electronic devices by patterning rows of holes in a large piece of graphene avoiding complete cutout and glued together, which might be beneficial for the integration of future graphene-based electric circuits. On experimental side, the patterned graphene nanostructures discussed here can be obtained experimentally by using techniques such as templated self-assembly of block copolymers¹³ or direct writing using a helium ion beam.¹⁴ The periodically patterned structure may be formed by first forming resist patterns on the graphene sheet followed by templated self-assembly of block copolymers in the region where the resist have been removed and etching of graphene by using the copolymer patterns as the mask. On the other hand, the random patterns can be formed by direct writing using a helium ion beam. Prior to the lithography processes, an alignment mark may be formed on the wafer by using an appropriate graphene edge as a reference so as to align the patterns in specific directions with respect to the underlying graphene lattice structure.

At last, we show a FET completely made of ZGNRs as shown in Fig. 5. In all previous theoretically proposed GNR-based FETs, the AGNR is an indispensable component due to the fact that pure ZGNR is metallic. Here, the proposed FET consists of two pure ZGNR electrodes (left and right), and a ZGNR with a defective (2, 2, 2, 2) edge structure. The transport calculations were done using a first principles approach combining the non-equilibrium Green's function's techniques and DFT via the ATK code.¹⁵⁻¹⁷ In the inset of the figure, the current-voltage (I-V) curve is shown for the zero gate voltage. The bias range of the zero current comes from the bandgap of the defective ZGNR in the center,

confirming the bandgap opening condition we derived from the tight binding approach. The currents as a function of gate voltage for different bias voltages suggest that the on-off ratio of this proposed FET is bigger than 1000. Compared to the previously proposed all-GNR based FET that used two ZGNRs and one AGNR,⁹ the FET suggested here has two obvious advantages: First, the complicated contacts between differently orientated AGNR and ZGNRs are avoided. Second, the precise control of ribbon width is not required.

III. CONCLUSION

In conclusion, using the tight-binding approach, we derived a general boundary condition for the band gap opening in the ZGNRs with defective edges: When the number of A-site defects equals to that of B-site defects, the ZGNRs are semiconducting. We further showed that the semiconducting ZGNRs generated this way can be integrated in a large piece of graphene by correctly patterning holes, which may be useful for the future large-scale integration of GNR-based devices. At last, we demonstrated using first principles calculations a high-performance FET completely made of ZGNRs. Results presented in this paper may be used to explain the recent experimental measurements showing that the transport gap always exists independent of the crystallographic orientations of GNRs. We expect these findings to provide impetus for new experiments as well motivations for new ideas in designing ZGNR-based electronic devices.

IV. ACKNOWLEDGMENT

We thank Professor A. H. Castro Neto and Dr. V. M. Pereira for stimulating and helpful discussions. This work was supported by NUS Academic Research Fund (Grant Nos: R-144-000-237133 and R-144-000-255-112). Computations were performed at the Centre for Computational Science and Engineering at NUS.

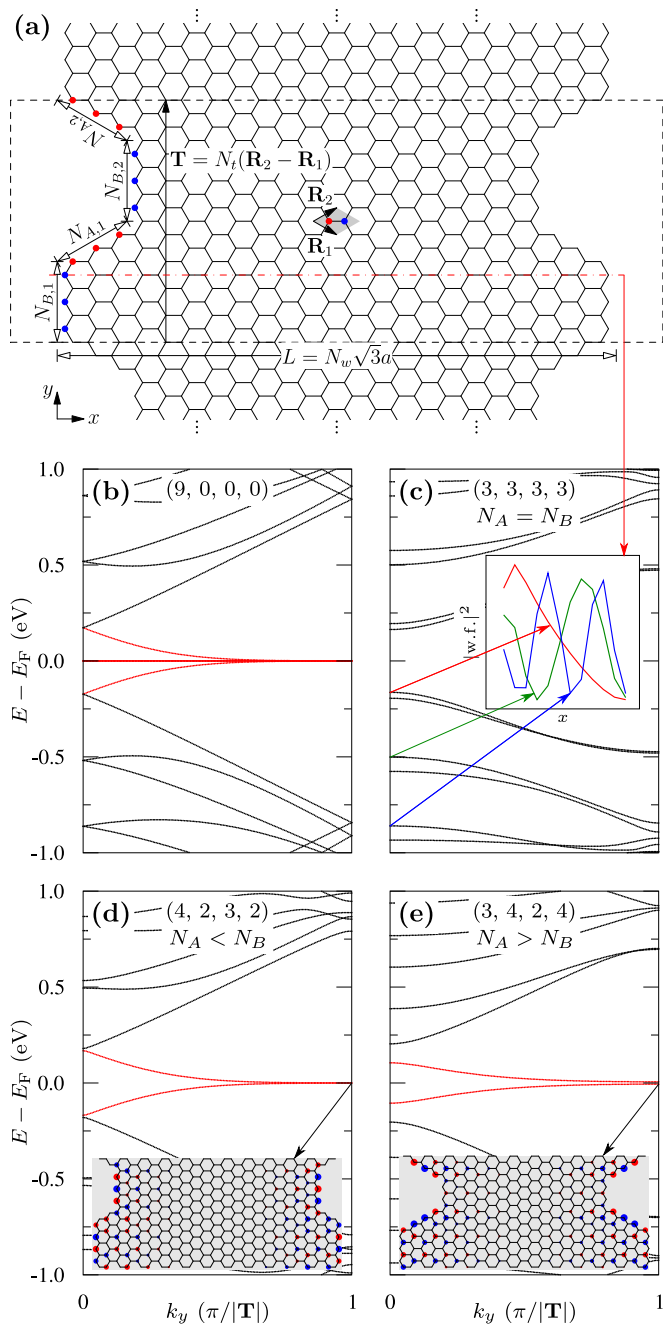


FIG. 1: (a) The lattice structure of a zigzag graphene nanoribbon with periodic edge structures. The unit cell is indicated by the dashed line. The edge structure is denoted by a quadruple of $(N_{B,1}, N_{A,1}, N_{B,2}, N_{A,2})$, each number of which corresponds to the segment length in unit of the graphene lattice constant, a . Other parameters of the system are the nanoribbon width (L) and the translational vector (\mathbf{T}). Carbon atoms belonging to different sublattices at edge are designated red (A) and blue (B) colors. (b-e) The band structures of nanoribbons with different edge structures and the same width $L = 12\sqrt{3}a$. In the inset of (c) are shown the squared wave functions along the dash-dotted line in (a) for different states at $k_y = 0$. The squared wave functions corresponding to the valence band maximums are also plotted in the insets of (d) and (e). The radii of filled discs are proportional to $R(\log_{10} |\psi(\mathbf{r})|^2 + 4)$, where $R(x)$ is the ramp function, and the color is determined by the sign of real part of $\psi(\mathbf{r})$.

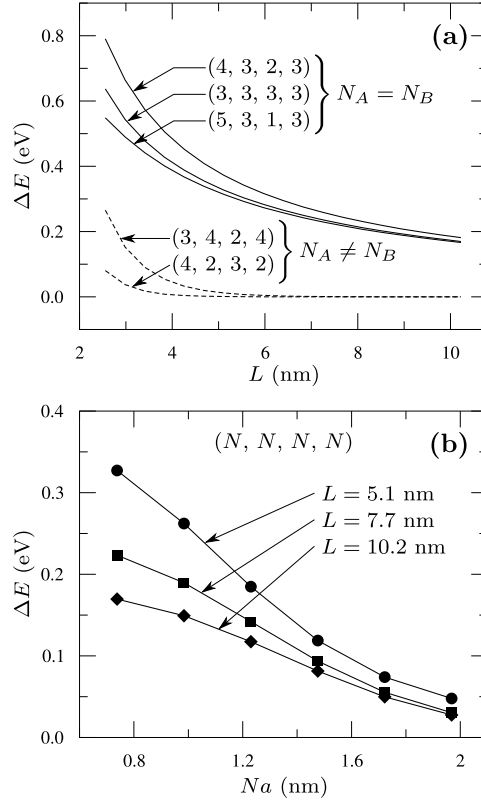


FIG. 2: (a) The variation of bandgaps as a function of the nanoribbon width (L) for different edge structures. (b) The variation of bandgaps as a function of the segment length (Na) of a (N, N, N, N) edge structure for different widths.

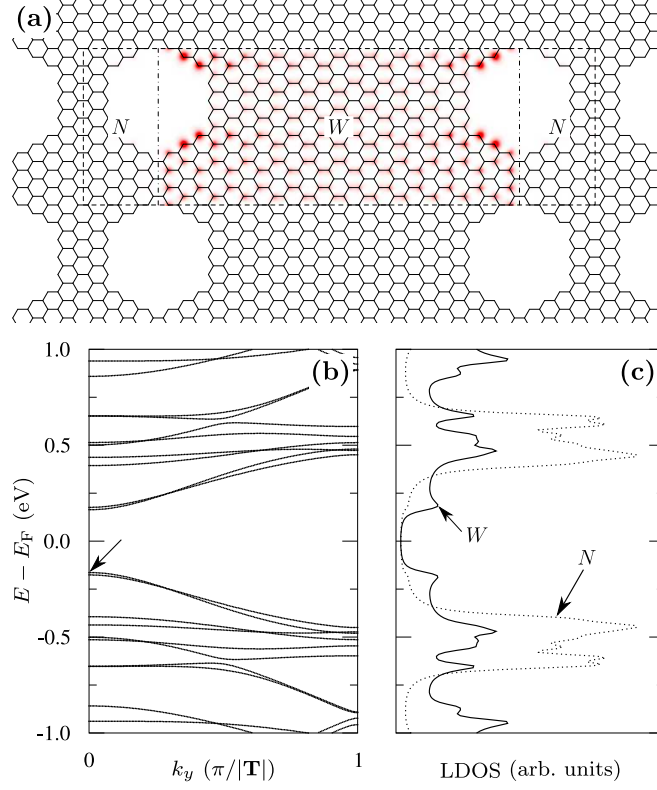


FIG. 3: (a) The unit cell (dashed line) of a wide nanoribbon (W) joined with a narrow nanoribbon (N) having the same edge structure. The nanoribbon W between two dash-dotted lines is identical to the nanoribbon shown in Fig. 1(a). (b) The band structure of the system in (a). The squared wave function plotted in (a) corresponds to the state indicated by an arrow. (c) The corresponding local density of states in W and N as shown in (a).

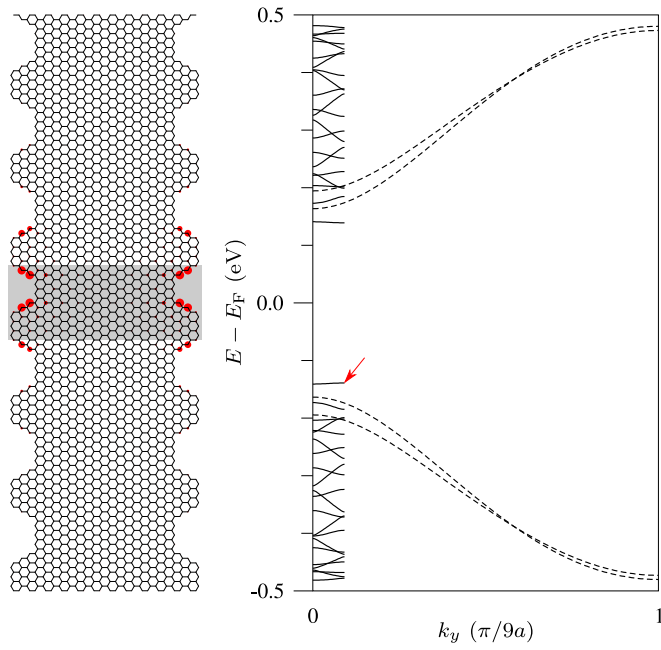


FIG. 4: The comparison between band structures of graphene nanoribbons with a pure (3, 3, 3, 3) edge structure (dashed line) and with one (3, 3, 2, 3) unit (as shaded) plus ten (3, 3, 3, 3) units in a supercell (solid line). The squared wave function (only part of the supercell is depicted) shown in the left panel suggests that the corresponding state (as arrowed) is localized around the defective (3, 3, 2, 3) unit.

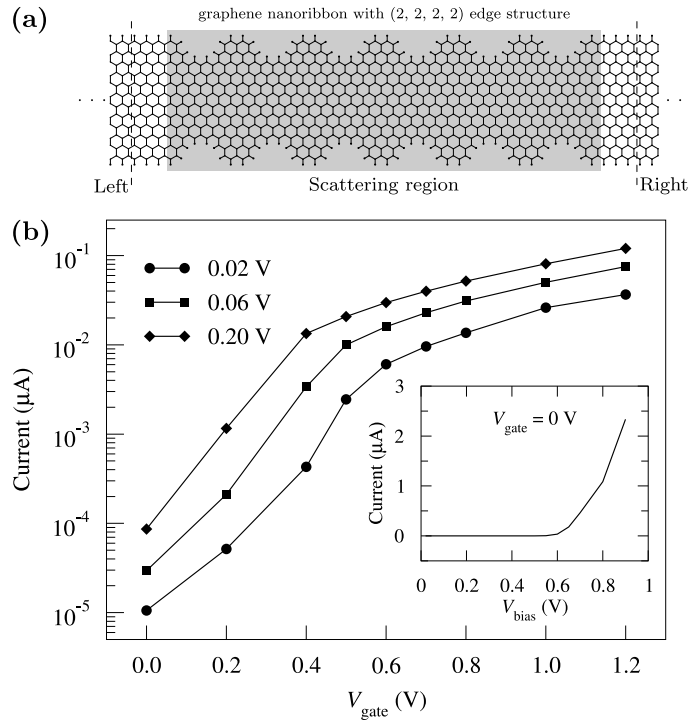


FIG. 5: (a) The configuration for the transport calculation. (b) The variation of current as a function of gate voltage for different bias voltages. The inset shows the bias voltage dependence of current for zero gate voltage.

* Electronic address: phyzc@nus.edu.sg

¹ K. S. Novoselov, A. K. Geim, S. V. Morozov, D. Jiang, Y. Zhang, S. V. Dubonos, I. V. Grigorieva, and A. A. Firsov, *Science* **306**, 666 (2004).

² K. S. Novoselov, A. K. Geim, S. V. Morozov, D. Jiang, M. I. Katsnelson, I. V. Grigorieva, S. V. Dubonos, and A. A. Firsov, *Nature* **438**, 197 (2005).

³ A. K. Geim and K. S. Novoselov, *Nat. Mater.* **6**, 183 (2007).

- ⁴ J. M. Cai, P. Ruffieux, R. Jaafar, M. Bieri, T. Braun, S. Blankenburg, M. Muoth, A. P. Seitsonen, M. Saleh, X. L. Feng, et al., *Nature* **466**, 470 (2010).
- ⁵ K. Nakada, M. Fujita, G. Dresselhaus, and M. S. Dresselhaus, *Phys. Rev. B* **54**, 17954 (1996).
- ⁶ Y.-W. Son, M. L. Cohen, and S. G. Louie, *Phys. Rev. Lett.* **97**, 216803 (2006).
- ⁷ S. Ihnatsenka, I. V. Zozoulenko, and G. Kirczenow, *Phys. Rev. B* **80**, 155415 (2009).
- ⁸ A. R. Akhmerov and C. W. J. Beenakker, *Phys. Rev. B* **77**, 085423 (2008).
- ⁹ Q. M. Yan, B. Huang, J. Yu, F. W. Zheng, J. Zang, J. Wu, B. L. Gu, F. Liu, and W. H. Duan, *Nano Lett.* **7**, 1469 (2007).
- ¹⁰ M. Y. Han, B. Özyilmaz, Y. Zhang, and P. Kim, *Phys. Rev. Lett.* **98**, 206805 (2007).
- ¹¹ T. G. Pedersen, C. Flindt, J. Pedersen, N. A. Mortensen, A.-P. Jauho, and K. Pedersen, *Phys. Rev. Lett.* **100**, 136804 (2008).
- ¹² A. H. Zhang, H. F. Teoh, Z. X. Dai, Y. P. Feng, and C. Zhang, *Appl. Phys. Lett.* **98**, 023105 (2011).
- ¹³ J. Y. Cheng, C. A. Ross, H. I. Smith, and E. L. Thomas, *Adv. Mater.* **18**, 2505 (2006).
- ¹⁴ M. C. Lemme, D. C. Bell, J. R. Williams, L. A. Stern, B. W. H. Baugher, P. Jarillo-Herrero, and C. M. Marcus, *ACS Nano* **3**, 2674 (2009).
- ¹⁵ J. Taylor, H. Guo, and J. Wang, *Phys. Rev. B* **63**, 245407 (2001).
- ¹⁶ M. Brandbyge, J.-L. Mozos, P. Ordejón, J. Taylor, and K. Stokbro, *Phys. Rev. B* **65**, 165401 (2002).
- ¹⁷ J. M. Soler, E. Artacho, J. D. Gale, A. García, J. Junquera, P. Ordejón, and D. Sánchez-Portal, *J. Phys.-Condes. Matter* **14**, 2745 (2002).